PAPER

Check for updates

Photo-oxidative degradation of methylammonium lead iodide perovskite: mechanism and protection†

Yixin Ouyang,[a] Yajuan Li,[b] Pengchen Zhu,[c] Qiang Li,[a] Yuan Gao,[c] Jianyu Tong,[d] Li Shi,[a] Qionghua Zhou,[a] Chongyi Ling, [ID][a] Qian Chen, [ID][a] Zhengtao Deng, [ID][d] Hairen Tan,[c] Weiqiao Deng [ID]*[b] and Jinlan Wang [ID]*[a]

Although the power conversion efficiency of perovskite solar cells has exceeded 23%, the poor ambient stability of organic–inorganic halide perovskites poses a challenge for their commercialization. Comprehensive understanding of the underlying degradation mechanisms is a crucial step to seek approaches that can effectively suppress the degradation of perovskites. Herein, on the basis of extensive first-principles calculations, a three-step photo-oxidative degradation mechanism of MAPbI$_3$ at the atomic level is revealed. We find that, in a dry ambient environment, the photo-generated superoxide anions (O$_2^-$) first lead to fast surface oxidation. However, further oxidation of the perovskite interior is hindered by the solid oxidation product. The fresh water produced in surface oxidation leads to the hydration of the inner perovskite and eventual breakage of the MAPbI$_3$ lattice. We devise a practical strategy for protecting MAPbI$_3$ from photo-induced decomposition by anchoring hydrophobic 2-(4-fluorophenyl)propan-2-amine on the surface of MAPbI$_3$. The surface modification significantly retards the photo-induced decomposition.

Organic–inorganic lead halide perovskites, as one of the most promising thin-film solar cell materials, have attracted intensive attention in photovoltaic manufacturing.[1–7] The remarkable photoelectric properties of perovskites, including tunable band gap, high extinction coefficient, and high carrier mobility,[8–10] led to over 23% power conversion efficiency (PCE).[11,12] However, the poor stability of perovskites under ambient conditions limits their practical applications severely.[13–17] Numerous experiments have revealed that moisture is the key culprit in the degradation of hybrid perovskites, for example, MAPbI$_3$. Meanwhile, hydrated perovskite phases, CH$_3$NH$_3$PbI$_3$·H$_2$O and (CH$_3$NH$_3$)$_4$PbI$_6$·2H$_2$O, have been observed during the initial hydration degradation process.[18–22] Theoretical calculations have demonstrated that water molecules can spontaneously incorporate into the perovskite lattice and gradually corrode the whole perovskite structure.[23,24]

Recent studies showed that degradation caused by light and oxygen occurred more rapidly than moisture-induced degradation.[25–30] When exposed to both light and dry air, MAPbI$_3$ suffered from rapid decomposition.[25,26] Calculations based on density functional theory suggested that PbO was the main photo-oxidation product rather than PbI$_2$.[27] The generation of PbO was later experimentally detected in degraded perovskites. However, PbI$_2$ was still the dominant composition whereas PbO was present as a by-product in a minimal amount.[28] So far, the degradation mechanism of hybrid perovskites under exposure to light and air remains unclear.

Tremendous efforts have been devoted to improving the stability of perovskite materials and photovoltaic devices. Hydrophobic hole- or electron-transporting materials, such as polymers, Al$_2$O$_3$, NiO$_x$ and carbon materials, have been widely employed as protective layers by encapsulation methods to meliorate the stability of perovskite solar cells.[31–33] Another strategy is to develop perovskite materials that have a two-dimensional layered structure by introducing large-sized hydrophobic molecules.[34–36] More recently, through functionalizing the perovskite surface by "moisture resistive" passivation molecules, superior moisture stability and high power conversion efficiency have been simultaneously achieved under a relatively high humidity.[37,38] Although these protection strategies are effective in suppressing the sensitivity of perovskites to moisture,

aSchool of Physics, Southeast University, Nanjing 211189, China. E-mail: jlwang@seu.edu.cn

bState Key Laboratory of Molecular Reaction Dynamics, Dalian Institute of Chemical Physics, Chinese Academy of Sciences, Dalian 116023, China. E-mail: dengwq@dicp.ac.cn

cNational Laboratory of Solid State Microstructures, Collaborative Innovation Centre of Advanced Microstructures, Jiangsu Key Laboratory of Artificial Functional Materials, College of Engineering and Applied Sciences, Nanjing University, Nanjing 210093, China

dDepartment of Biomedical Engineering, College of Engineering and Applied Sciences, Nanjing National Laboratory of Microstructures, Collaborative Innovation Center of Advanced Microstructures, Nanjing University, Nanjing 210093, China

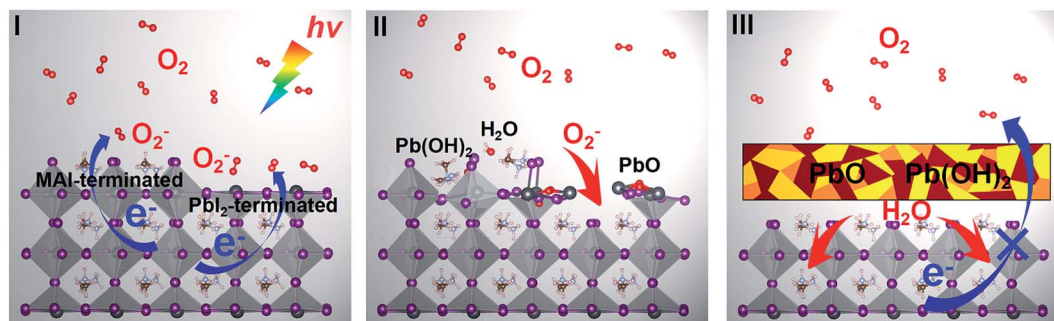† Electronic supplementary information (ESI) available. See DOI: 10.1039/c8ta12193a

This journal is © The Royal Society of Chemistry 2019

J. Mater. Chem. A, 2019, 7, 2275–2282 | 2275

Fig. 1 Schematic representation of the photo-oxidative degradation process of the MAPbI$_3$ (001) surface. Step I: the O$_2$ close to the surface of MAPbI$_3$ gets the photo-excited electrons from MAPbI$_3$, forming O$_2^-$. Step II: O$_2^-$ reacts with [CH$_3$NH$_3$]$^+$ and Pb, yielding H$_2$O and Pb(OH)$_2$ on the MAI-terminated surface. Oxidation of Pb on the PbI$_2$-terminated surface leads to the disintegration of the Pb–I bond. Then the underlying MAI-terminated surface is exposed. Step III: the oxidation products prevent the oxidation of inner MAPbI$_3$. Then, the fresh water molecules produced in surface oxidation cause hydration of the inner perovskite and eventually break down the perovskite.

approaches that can retard the photo-oxidation and hydration of perovskites have been little investigated.

In this work, we provide a comprehensive understanding on the photo-oxidation mechanism of MAPbI$_3$ under ambient conditions. Our calculations reveal that the photo-induced degradation process includes three key steps: generation of superoxide on the surface under light, fast oxidation of the MAPbI$_3$ surface and production of water, and slow hydration of inner MAPbI$_3$ (Fig. 1). A rational design of the protection strategy is devised from first-principles methods and is verified by stability tests from experiments. We show that modifying the surface of MAPbI$_3$ with 2-(4-fluorophenyl)propan-2-amine (FPA) can suppress the photo-corrosion due to oxygen and water.

Results and discussion

We first investigate the interaction between oxygen and MAPbI$_3$. There exist two typical crystal structures of the MAPbI$_3$ perovskite: the tetragonal phase at room temperature and the orthorhombic phase at low temperature (<162 K).[39] Meanwhile, the (001) surface, which is the main framework of the bulk, is considered as one of the most common surfaces of the perovskite and it can be either MAI or PbI$_2$-terminated (S$_{MA-I}$ and S$_{Pb-I}$).[40,41] Therefore, MAPbI$_3$ in the tetragonal phase and both MAI and PbI$_2$-terminated (S$_{MA-I}$ and S$_{Pb-I}$) surfaces are considered in this study (the structure of the tetragonal phase and slab models of different surfaces are displayed in ESI Fig. 1 and 2,† respectively). The adsorption energies of O$_2$ on the six adsorption sites (see Fig. 2a and ESI Fig. 3 and 4†) are presented in Table 1. On the S$_{Pb-I}$ surface, the adsorption energies of the hollow site and Pb-top site are 0.14 and 0.11 eV, suggesting a weak interaction between O$_2$ and the surface. On the MAI-terminated surface, the adsorption energies of all sites are close to zero, indicating that the interaction between O$_2$ and the S$_{MA-I}$ surface is also very weak.

Next, we study the influence of O$_2$ on the stability of the MAPbI$_3$ (001) surface by AIMD simulations and the structure evolution of clean S$_{Pb-I}$ and S$_{MA-I}$ at 300 K in 3 ps is calculated as a reference. As shown in Fig. 2b and c, the Pb–I frameworks of S$_{Pb-I}$ and S$_{MA-I}$ are slightly distorted at 300 K, but no major

damage is observed on both surfaces, and the octahedron PbI$_6$ cages still exist. When the surfaces are exposed to oxygen, the O$_2$ is captured by S$_{Pb-I}$ (either Pb-top or hollow site) but free-floating on S$_{MA-I}$, consistent with the above adsorption energy results. More importantly, both S$_{Pb-I}$ and S$_{MA-I}$ maintain their structural integrity in an oxygen-rich environment, indicating that O$_2$ alone does not degrade the perovskite solar cell. This agrees well with the experimental observation that perovskite solar cells are stable for prolonged periods of time in dry air in the dark.[42]

It has been reported that MAPbI$_3$ rapidly decomposes when it is exposed to light and dry air.[25,26,28] The superoxide is suggested as the culprit that triggers the degradation.[26] In general, a light and oxygen-induced reaction highly depends on the band structure of the reactants; more specifically, the semiconductor absorber should have a suitable band gap and well-matched band edges to the redox potential of O$_2$/O$_2^-$.[43] Fig. 3a depicts the band structure of MAPbI$_3$ with respect to the vacuum level. The suitable direct band gap makes MAPbI$_3$ produce enough excitons under ambient light. Meanwhile, the redox potential of O$_2$/O$_2^-$ is just located inside the band gap. Thus, the photo-generated electrons can quickly transfer from the conduction band of MAPbI$_3$ to the O$_2$ on the surfaces, which leads to the formation of superoxide anions O$_2^-$. The formed O$_2^-$ physisorbs on the surfaces of MAPbI$_3$ with a stronger adsorption than that of the neutral O$_2$ (0.64 eV vs. 0.11 eV on S$_{Pb-I}$ and 0.63 eV vs. 0.05 eV on S$_{MA-I}$, as listed in Table 1; detailed adsorption configurations are given in ESI Fig. 5 and 6†). The stronger adsorption of O$_2^-$ results from its electrostatic attraction towards Pb^{2+} and [CH$_3$NH$_3$]$^+$.

We now consider the reaction of O$_2^-$ with MAPbI$_3$ and how the reaction leads to the decomposition of MAPbI$_3$. On the PbI$_2$-terminated surface, with O$_2^-$ approaching the Pb–I frameworks, the O–O bond is enlarged and Pb–O chemical bonds are formed. Due to the higher electronegativity of oxygen compared to iodine, the O atoms prefer to replace adjacent I atoms and bond to two Pb atoms. As shown in Fig. 4a, the energy barrier for dissociating O$_2^-$ on S$_{Pb-I}$ is 0.79 eV, indicating that this process can occur at a moderate temperature of about 330 K (estimated from transition-state theory, $10^{12} \exp(-E_b/kT) \approx 1$, where $E_b =$

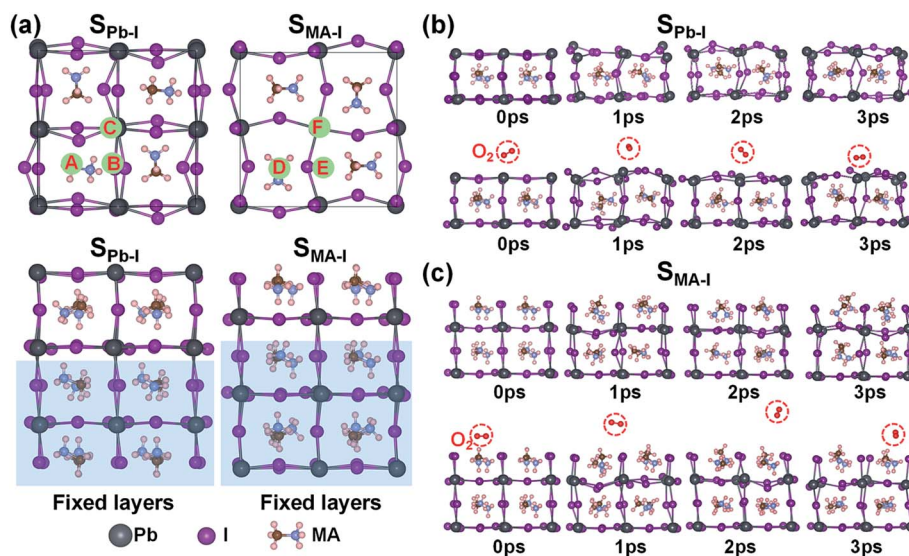**Fig. 2** (a) Side and top views of slab models of PbI_2- and MAI-terminated (001) surfaces (S_{Pb-I} and S_{MA-I}) of $MAPbI_3$. The layers inside the blue rectangle regions are fixed to bulk positions while other layers are relaxed. The green balls indicate the six different adsorption sites of O_2, O_2^- and H_2O. Structure evolutions of (b) clean S_{Pb-I} and S_{Pb-I} with O_2 adsorption and (c) clean S_{MA-I} and S_{MA-I} with O_2 adsorption at 300 K obtained from AIMD simulations. The O_2 molecules are marked with red circles.

Table 1 Calculated adsorption energies (unit in eV), E_{ad} (eV), of O_2 and O_2^- on the (001) surface of $MAPbI_3$

	PbI₂-terminated surface (S_{Pb-I})			MAI-terminated surface (S_{MA-I})		
	Hollow (site A)	I-top (site B)	Pb-top (site C)	MA-top (site D)	Hollow (site E)	I-top (site F)
O_2	0.14	0.06	0.11	0.05	−0.02	−0.09
O_2^-	0.23	0.55	0.64	0.44	0.63	0.04

0.79 eV). In fact, the MAPbI₃ is hole-doped by light excitation. The strong Coulomb interaction between O_2^- and hole-doped $MAPbI_3$ is not included in our calculation. In other words, the

reaction barrier could be even lower in real situations. In addition, our AIMD simulations further demonstrate that the transformation of O_2^- from physisorption to chemisorption on S_{Pb-I} occurs rapidly at room temperature (see Fig. 4b). The formation of Pb–O bonds leads to the gathering of Pb and O atoms and the formation of lead oxide. I atoms in the inorganic frameworks are replaced by the O atoms and tend to form volatile iodine (I_2) (ESI Fig. 8a†). As a consequence, serious breakage is introduced into the Pb–I frameworks and the underlying MAI-terminated surface is exposed.

In the case of the MAI-terminated surface, there exist two possible reaction pathways according to the affinity of O_2^- towards the $[CH_3NH_3]^+$ cation or Pb^{2+} cation. On one hand, one O atom of O_2^- takes two H atoms from adjacent $[CH_3NH_3]^+$
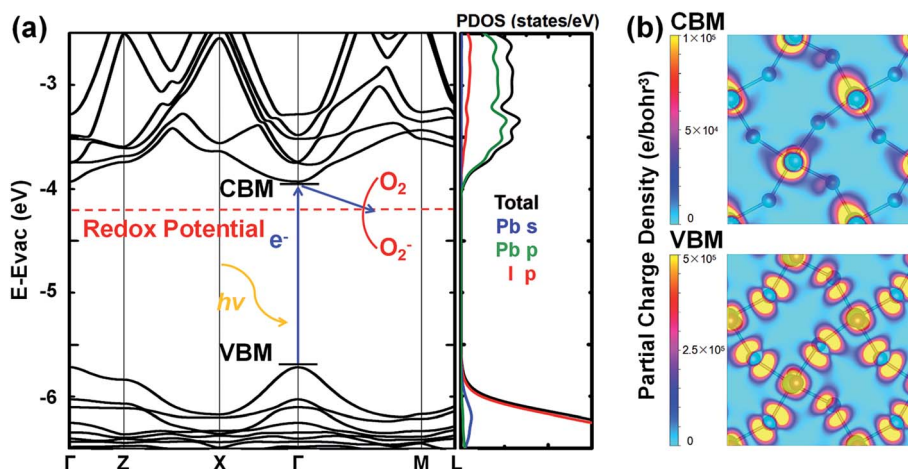

Fig. 3 (a) Band structure and projected density of states for $MAPbI_3$. The CBM of $MAPbI_3$ and redox potential of O_2/O_2^- with respect to the vacuum energy are −3.9 eV and −4.2 eV,[5,43] respectively. (b) Partial charge density plots for the CBM and VBM of $MAPbI_3$. The CBM is dominated by the p orbitals of Pb atoms, and the VBM is dominated by the coupling between the s orbitals of Pb atoms and the p orbitals of I atoms.
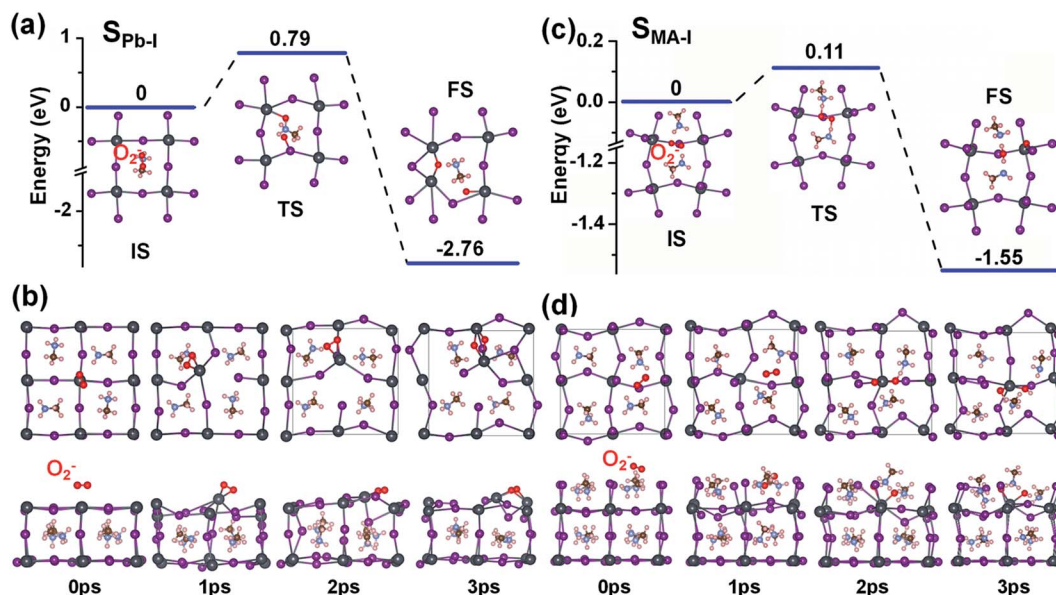
This journal is © The Royal Society of Chemistry 2019

J. Mater. Chem. A, 2019, **7**, 2275–2282 | **2277**

Fig. 4 Reaction path for O_2^- adsorbed on (a) the PbI_2-terminated surface and (c) MAI-terminated surface from physisorption to chemisorption. Snapshots of AIMD simulations of O_2^- on (b) the PbI_2-terminated surface and (d) MAI-terminated surface at a temperature of 300 K.

cations, forming a water molecule with an energy barrier of 0.11 eV. Another O atom adsorbs on the adjacent Pb (see Fig. 4c). In this pathway, all the $[CH_3NH_3]^+$ on the surface will convert into water and volatile methylamine. The formation of Pb–O bonds will result in disintegration of the local Pb–I octahedral structure (ESI Fig. 8b†). On the other hand, the O_2^- anion bonds with one Pb atom and takes two H atoms from adjacent $[CH_3NH_3]^+$, forming the precursor of $Pb(OH)_2$ (see Fig. 4d). Subsequently, the unstable $Pb(OH)_2$ further decomposes into PbO and H_2O.[22] In summary, the O_2^- reacts with $MAPbI_3$ by attaching to the cations in $MAPbI_3$, *i.e.*, Pb^{2+} and $[CH_3NH_3]^+$, forming lead oxide and water which induce the structural collapse of $MAPbI_3$.

The above discussions suggest that the solid oxidation products of $MAPbI_3$ should mainly be PbO on the surface. However, PbI_2 is typically detected as the dominant product of degradation in light and a dry air environment.[25,26,28] The oxidation products on the surface could potentially serve as a protection layer to stop further oxidation. For example, black phosphorous and InSe can be protected by fully oxidized layers on the surface.[43,44] In the case of $MAPbI_3$, the oxidation products PbO and $Pb(OH)_2$, on one hand, as wide band-gap semiconductors in the bulk phase (>2.5 eV),[45,46] can obstruct the transfer of photo-excited electrons from the perovskite to molecular oxygen, avoiding the formation of superoxide. On the other hand, they may serve as a protection layer to prevent further penetration of O_2 and H_2O from the air environment. Hence, the O_2^- concentration would decrease rapidly and the oxidation degradation would be gradually terminated. However, the fresh H_2O molecules, which are produced in surface oxidation, have strong affinity towards the cations of $MAPbI_3$ and give rise to continuous hydration degradation of inner $MAPbI_3$.

To verify this point, we made further room-temperature AIMD simulations by constructing a model of lead oxide covered $MAPbI_3$. As shown in Fig. 5, the O_2 and H_2O from the air environment are completely isolated from the $MAPbI_3$ by the PbO film. During the simulation time, O_2 and H_2O adsorb near the surface of the PbO film. Meanwhile the oxide monolayer maintains its integrity with no O_2 or H_2O penetrating into the
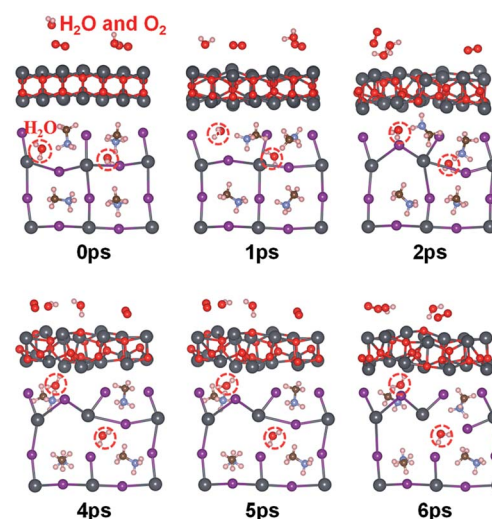

Fig. 5 Room temperature AIMD simulations were performed on the lead oxide covered $MAPbI_3$ surrounded by H_2O and O_2 on the surface and H_2O in the inside. The H_2O and O_2 molecules in the ambient environment are fully separated by lead oxide. But the water molecules produced in the reaction between superoxide and methylammonium permeate into the inner of $MAPbI_3$ and gradually corrode the crystal structure of $MAPbI_3$. The water molecules in $MAPbI_3$ are marked with red circles.

$MAPbI_3$. Nevertheless, the fresh H_2O produced in the surface oxidation can penetrate into the inner of $MAPbI_3$ owing to the large interspace between inorganic frameworks and organic molecules. Structural collapse of inorganic frameworks induced by H_2O is observed after about 4 ps, which is much slower than that caused by oxidation as observed in experiments.[25] This suggests that oxidation occurs fast on the $MAPbI_3$ surface and forms a surface-covering layer of PbO. Meanwhile the inner degradation dominated by generated H_2O occurs slowly, yielding a large amount of PbI_2. Hence, lead iodide, as the principal product of hydration degradation, is therefore detected in degraded $MAPbI_3$,[19,20,25,26] whereas the oxidation intermediate, *i.e.*, lead oxide, can only be detected as a by-product by X-ray photoemission spectroscopy (XPS).[28]

Now, we have a comprehensive picture of the light and oxygen-induced degradation of $MAPbI_3$. First, superoxide anions are generated through a charge transfer reaction on the surface of $MAPbI_3$ under ambient light. Then, the highly active superoxide anions react with the $MAPbI_3$ surface: (i) the oxidation of the PbI_2-terminated surface leads to the formation of PbO and serious breakage of the surface with the underlying MAI-terminated surface exposed and (ii) the exposed MAI-terminated surface is further oxidized to PbO and H_2O or the unstable $Pb(OH)_2$. Third, the oxidation products PbO and $Pb(OH)_2$ serve as a protection layer to prevent the further oxidation of inner $MAPbI_3$. Nevertheless, the fresh H_2O molecules produced in the reaction of superoxide with methylammonium and the decomposition of $Pb(OH)_2$ act as active species, cause hydration of the inner perovskite and ultimately destroy the $MAPbI_3$. Therefore, we can conclude that the light and oxygen-induced degradation of $MAPbI_3$ is accomplished through a rapid surface oxidation triggered by the superoxide anions and a slow inner hydration degradation caused by the fresh water molecules produced in the surface oxidation. The proposed degradation processes provide a good understanding of very recent experimental observations. Haque *et al.* found that the device performance of perovskite solar cells degraded in a matter of hours in a dry ambient environment, whereas structural degradation from $MAPbI_3$ to PbI_2 occurred on a timescale of days.[25] In light of our proposed mechanism, the rapid degradation of the device performance is caused by the surface oxidation, and the slow structural degradation from $MAPbI_3$ to PbI_2 is caused by the inner hydration. In the film of $MAPbI_3$, the surfaces of $MAPbI_3$ nanoparticles exposed to oxygen are oxidized, with the oxidation products adhering to the grains. The oxidized surfaces impede the charge transport within the perovskite film and the charge extraction from the perovskite to transport layers, which ultimately leads to the decrease of photovoltaic performance in a matter of hours. However, with the rapid depletion and diminishing superoxide generation, the oxidation degradation gradually stops. Thereafter, the H_2O molecules generated from the surface oxidation slowly corrode the inner of $MAPbI_3$ on a timescale of days. The experimental work of Vaynzof *et al.* also provides strong support to our degradation process of fast surface oxidation and slow inner hydration.[28] By X-ray photoemission spectroscopy, they found just a small amount of oxidation products such as lead

oxide on the surface. The hydration products such as lead iodide were still the principal degradation products. Note that although we clarify the fundamental light and oxygen-induced degradation mechanism here, there are still a lot of questions worth exploring. For example, how does one understand the roles of surface defects and grain boundaries in oxygen induced degradation?

From the above discussion, we have known that the superoxide anions and water molecules are two key factors for the degradation of $MAPbI_3$. Thus, both O_2^- and H_2O should be isolated to protect $MAPbI_3$ against the ambient environment. For the oxidation process, the production of O_2^- can be restricted by extracting photo-excited electrons from the $MAPbI_3$ using either conducting scaffolds or high performance compact electrode interface layers.[29] However, to fully extract photo-excited electrons, the solar cell requires working conditions at maximum operating voltages,[29] which greatly reduces the power conversion efficiency of $MAPbI_3$. Surface modification benefits from facile preparation and low cost for large-scale production compared with common encapsulation methods. It has been proven to be an effective method against a H_2O-rich environment. Meanwhile, a high photoelectric conversion efficiency is maintained.[34,35] It is crucial to find an appropriate substitute for methylammonium to modify the surface of $MAPbI_3$ to achieve excellent moisture and oxygen tolerance simultaneously. For this purpose, benzylamine (BA) and 2-(4-fluorophenyl)propan-2-amine (FPA) are chosen to substitute the methylammonium on the (001) surface of $MAPbI_3$ (see Fig. 6a).

It has been proven that substituting methylammonium with BA can efficiently improve the moisture resistance of the perovskite,[38] but could it make perovskite immune to photo-oxidation as well? As shown in Fig. 6b, the diffusion barrier of oxygen molecules from the BA-modified surface to Pb–I frameworks is 0.73 eV, indicating that the oxygen in air can still cross the interspace between benzylamine at room temperature. Once the oxygen is close enough to the Pb–I frameworks, it can get photo-generated electrons and be reduced to O_2^-, and then oxidation of Pb–I frameworks will quickly occur and lead to the breakdown of $MAPbI_3$ (ESI Fig. 10b†). For the replacement with FPA, due to the suitable size of FPA, a dense protective layer is constructed, which contains numerous inert groups. The energy barrier for O_2 diffusing from the FPA-modified surface to Pb–I frameworks increases up to 1.56 eV (Fig. 6c). Thus the dense layer could effectively avoid O_2 reaching the Pb–I frameworks, which suppresses the generation of O_2^-. In addition, the exposed hydrophobic groups of FPA endow the FPA-substituted surface with good hydrophobicity (ESI Fig. 11†). Obviously, the weak van der Waals interaction between FPA and Pb–I frameworks will not affect the intrinsic property of the inner perovskite. Instead, the π-conjugation structure of FPA can facilitate the charge transport between $MAPbI_3$ and charge transport materials. Therefore, the high air resistance of $MAPbI_3$ can be expected by means of FPA modification, while the outstanding photophysical properties remain unaffected.

Inspired by the findings from DFT calculations, we then experimentally investigated the effect of BA and FPA modification on the stability of $MAPbI_3$. We first examined the $MAPbI_3$

This journal is © The Royal Society of Chemistry 2019

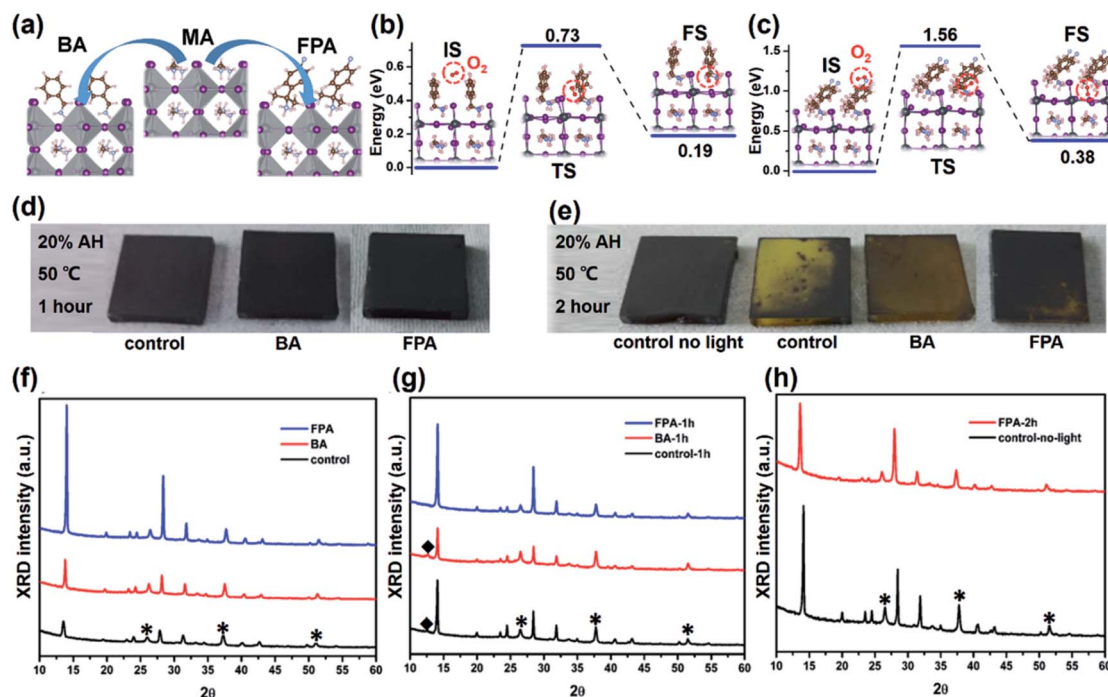*J. Mater. Chem. A*, 2019, **7**, 2275–2282 | **2279**

Fig. 6 (a) Schematic illustration of surface functionalization by replacing methylammonium with benzylamine (BA) and 2-(4-fluorophenyl) propan-2-amine (FPA). Diffusion path of O_2 into (b) BA and (c) FPA modified MAPbI$_3$. (d) Photos of the control film and BA and FPA modified films exposed to light and 20% air humidity (AH) for 1 h at 50 °C, respectively. (e) Photos of the control film without exposure to light and the control film and BA and FPA modified films exposed to light for 2 h, respectively. (f) XRD patterns of the control film and BA and FPA modified films before exposure to light, respectively. The characteristic peaks of FTO are marked with *. (g) XRD patterns of the control film and BA and FPA modified films exposed to light for 1 h, respectively. The characteristic peak of PbI$_2$ is marked with ◆. (h) XRD patterns of the control film without exposure to light and the FPA modified film exposed to light for 2 h, respectively.

film stability under light (100 mW cm^{-2}, 50 °C and 20% air humidity) by XRD measurements, as shown in Fig. 6. As shown in Fig. 6f, all the films exhibit tetragonal phase XRD patterns before exposure to light. After exposure to light for 1 h, the control film (without the protective layer) and BA modified film began to decompose and the films exhibit the peak of PbI$_2$ at 12.58° (Fig. 6g and h). However, the FPA modified film remained unchanged even after exposure to light for 2 h, comparable to the control film without exposure to light (Fig. 6h). However, the control film and BA modified film were totally decomposed to PbI$_2$ after exposure to light for 2 h, as shown in Fig. 6e. Compared to the control film without exposure to light, decomposition of the control film and BA modified film in short time is attributed to O_2^- caused by light illumination. Because of the close-packed arrangement of FPA, the FPA modified films show significantly improved stability against oxygen and water.

Conclusions

In summary, we have established a comprehensive picture of the photo-oxidative degradation of MAPbI$_3$ under ambient conditions and proposed an effective strategy to resist corrosion due to water and oxygen. The degradation includes three important steps: generation of superoxide anions under light illumination, rapid oxidation of the surface perovskite and

production of water, and slow hydration of the inner perovskite. The generation of the superoxide anions triggers the surface oxidation of MAPbI$_3$. The solid oxidation products form a protective layer to prevent the further oxidation of inner MAPbI$_3$. Meanwhile the fresh water molecules produced in surface oxidation will cause hydration of the inner perovskite and ultimate breakage of the perovskite. We further demonstrate that the replacement of methylammonium with 2-(4-fluorophenyl)propan-2-amine on the surface of MAPbI$_3$ can effectively prevent the infiltration of both water and oxygen, consequently avoiding the degradation of MAPbI$_3$. This study provides an in-depth understanding on the degradation mechanism of MAPbI$_3$ and opens a new avenue towards realizing the long-term stability of perovskite-based solar cells.

Methods

Density functional theory (DFT) calculations

All DFT calculations were performed using Vienna Ab initio Simulation Package (VASP).[47,48] The spin-polarized general gradient approximation in the Perdew–Burke–Ernzerhof (PBE)[49] form was used. van der Waals (vdW) interactions were considered for weak interaction cases using the semiempirical correction scheme of Grimme, DFT-D3.[50] The energy cutoff for the plane-wave basis set was set at 400 eV. The convergence

2280 | J. Mater. Chem. A, 2019, 7, 2275–2282

This journal is © The Royal Society of Chemistry 2019

threshold was 10^{-4} eV for energy and 0.02 eV Å^{-1} for force, respectively. The pseudopotential was scalar-relativistic and accounted partially for relativistic effects. The electronic structure was calculated without considering the spin–orbit coupling (SOC) to obtain a band gap consistent with experimental data. AIMD simulations were performed using the Nose–Hoover method[51] to control the temperature. The climbing-image nudged elastic band (CI-NEB) method[52] was employed to locate the minimum-energy path. The lattice parameters of bulk tetragonal MAPbI$_3$ were optimized using a Monkhorst–Pack k-mesh of a $5 \times 5 \times 3$ grid and a tetragonal unit cell containing 48 atoms (see ESI Fig. 1†). A periodical slab of two and half layers MAPbI$_3$ (001) surface is used to perform structural relaxation and AIMD simulations (see Fig. 2a and ESI Fig. 2†). A vacuum of at least 20 Å in the z-direction was used to avoid the interaction between two periodic units. The Brillouin zone of slabs was sampled by using a Monkhorst–Pack k-mesh of a $3 \times 3 \times 1$ grid and a $2 \times 2 \times 1$ grid for structural relaxation and AIMD simulations, respectively. The bottom of the slabs (inside the blue rectangle region in Fig. 2a) was fixed to their bulk positions during relaxation, while the rest of the layers were fully relaxed.

MAPbI$_3$ film fabrication

PbI$_2$ (Sigma-Aldrich), MAI (Xian P-OLED company), benzylamine (BA, TCI) and 2-(4-fluorophenyl)propan-2-amine (FPA, Apollo) were used as received. All the films were fabricated under an atmospheric environment (~20 °C, 30–40% air humidity). To obtain 1.45 M MAPbI$_3$ solution, PbI$_2$ and MAI powders were stirred in a mixture of DMSO and DMF (6 : 4) for 12 h. The resulting solution was coated onto an FTO substrate by a consecutive two-step spin-coating process at 1000 and 5000 rpm for 10 and 30 s, respectively. During the second spin-coating step, the substrate was treated with chlorobenzene drop-casting. The substrate was annealed on a hot plate at 100 °C for 10 min. For the modified film, 0.1 M BA and FPA chlorobenzene solution were dropped onto the MAPbI$_3$ substrate, immediately followed by spin coating at 3000 rpm for 30 s and then drying at 100 °C for 10 min. For the control film, only chlorobenzene solvent was dropped on the MAPbI$_3$ substrate.

Light experiments

The light experiment was performed using a Xenon Weather-Ometer under an atmospheric environment. The power of light was set at 100 mW cm^{-2}. During the light experiment, the temperature was limited below 50 °C, and the air humidity was about 20%.

Author contributions

J. W. conceived the project. Y. O. performed all calculations. Y. L., P. Z. and J. T. contributed to the synthesis of materials and the characterization. Y. O., Q. L., Y, L, W. D. and J. W. co-wrote the paper, with all authors contributing to the discussion and preparation of the manuscript.

Conflicts of interest

There are no conflicts to declare.

Acknowledgements

References

1 A. Kojima, K. Teshima, Y. Shirai and T. Miyasaka, *J. Am. Chem. Soc.*, 2009, **131**, 6050–6051.

2 M. Z. Liu, M. B. Johnston and H. J. Snaith, *Nature*, 2013, **501**, 395–398.

3 G. Hodes, *Science*, 2013, **342**, 317–318.

4 H. P. Zhou, Q. Chen, G. Li, S. Luo, T. B. Song, H. S. Duan, Z. R. Hong, J. B. You, Y. S. Liu and Y. Yang, *Science*, 2014, **345**, 542–546.

5 A. Y. Mei, X. Li, L. F. Liu, Z. L. Ku, T. F. Liu, Y. G. Rong, M. Xu, M. Hu, J. Z. Chen, Y. Yang, M. Gratzel and H. W. Han, *Science*, 2014, **345**, 295–298.

6 N. Cho, F. Li, B. Turedi, L. Sinatra, S. P. Sarmah, M. R. Parida, M. I. Saidaminov, B. Murali, V. M. Burlakov, A. Goriely, T. Wu and O. M. Bakr, *Nat. Commun.*, 2016, **7**, 13407.

7 L. Ma, J. Dai and X. Zeng, *Adv. Energy Mater.*, 2017, **7**, 1601731.

8 G. C. Xing, N. Mathews, S. Y. Sun, S. S. Lim, Y. M. Lam, M. Gratzel, S. Mhaisalkar and T. C. Sum, *Science*, 2013, **342**, 344–347.

9 F. Li, H. Wang, D. Kufer, L. Liang, W. Yu, E. Alarousu, C. Ma, Y. Li, Z. Liu and C. Liu, *Adv. Mater.*, 2017, **29**, 1602432.

10 A. Miyata, A. Mitioglu, P. Plochocka, O. Portugall, J. T. W. Wang, S. D. Stranks, H. J. Snaith and R. J. Nicholas, *Nat. Phys.*, 2015, **11**, 582–587.

11 B. Chen, Y. Bai, Z. Yu, T. Li, X. Zheng, Q. Dong, L. Shen, M. Boccard, A. Gruverman, Z. Holman and J. Huang, *Adv. Energy Mater.*, 2016, **6**, 1601128.

12 M. Saliba, T. Matsui, J. Y. Seo, K. Domanski, J. P. Correa-Baena, M. K. Nazeeruddin, S. M. Zakeeruddin, W. Tress, A. Abate, A. Hagfeldt and M. Gratzel, *Energy Environ. Sci.*, 2016, **9**, 1989–1997.

13 M. Long, T. Zhang, Y. Chai, C.-F. Ng, T. C. W. Mak, J. Xu and K. Yan, *Nat. Commun.*, 2016, **7**, 13503.

14 T. Leijtens, G. E. Eperon, N. K. Noel, S. N. Habisreutinger, A. Petrozza and H. J. Snaith, *Adv. Energy Mater.*, 2015, **5**, 1500963.

15 N. H. Tiep, Z. Ku and H. J. Fan, *Adv. Energy Mater.*, 2016, **6**, 1501420.

16 J. S. Manser, M. I. Saidaminov, J. A. Christians, O. M. Bakr and P. V. Kamat, *Acc. Chem. Res.*, 2016, **49**, 330–338.

This journal is © The Royal Society of Chemistry 2019

J. Mater. Chem. A, 2019, **7**, 2275–2282 | 2281

17 M. Long, T. Zhang, M. Liu, Z. Chen, C. Wang, W. Xie, F. Xie, J. Chen, G. Li and J. Xu, *Adv. Mater.*, 2018, **3**, 1801562.

18 J. A. Christians, P. A. Miranda Herrera and P. V. Kamat, *J. Am. Chem. Soc.*, 2015, **137**, 1530–1538.

19 J. M. Frost, K. T. Butler, F. Brivio, C. H. Hendon, M. van Schilfgaarde and A. Walsh, *Nano Lett.*, 2014, **14**, 2584–2590.

20 Z. Song, A. Abate, S. C. Watthage, G. K. Liyanage, A. B. Phillips, U. Steiner, M. Graetzel and M. J. Heben, *Adv. Energy Mater.*, 2016, **6**, 1600846.

21 A. M. A. Leguy, Y. Hu, M. Campoy-Quiles, M. I. Alonso, O. J. Weber, P. Azarhoosh, M. van Schilfgaarde, M. T. Weller, T. Bein, J. Nelson, P. Docampo and P. R. F. Barnes, *Chem. Mater.*, 2015, **27**, 3397–3407.

22 W. Huang, J. S. Manser, P. V. Kamat and S. Ptasinska, *Chem. Mater.*, 2016, **28**, 303–311.

23 E. Mosconi, J. M. Azpiroz and F. De Angelis, *Chem. Mater.*, 2015, **27**, 4885–4892.

24 C. J. Tong, W. Geng, Z. K. Tang, C. Y. Yam, X. L. Fan, J. Liu, W. M. Lau and L. M. Liu, *J. Phys. Chem. Lett.*, 2015, **6**, 3289–3295.

25 N. Aristidou, C. Eames, I. Sanchez-Molina, X. Bu, J. Kosco, M. S. Islam and S. A. Haque, *Nat. Commun.*, 2017, **8**, 15218.

26 N. Aristidou, I. Sanchez-Molina, T. Chotchuangchutchaval, M. Brown, L. Martinez, T. Rath and S. A. Haque, *Angew. Chem., Int. Ed.*, 2015, **54**, 8208–8212.

27 L. Zhang and P. H.-L. Sit, *J. Mater. Chem. A*, 2017, **5**, 9042.

28 Q. Sun, P. Fassl, D. Becker-Koch, A. Bausch, B. Rivkin, S. Bai, P. E. Hopkinson, H. J. Snaith and Y. Vaynzof, *Adv. Energy Mater.*, 2017, **7**, 1700977.

29 A. J. Pearson, G. E. Eperon, P. E. Hopkinson, S. N. Habisreutinger, J. T. W. Wang, H. J. Snaith and N. C. Greenham, *Adv. Energy Mater.*, 2016, **6**, 10.

30 X. MA and Z. Li, *Appl. Surf. Sci.*, 2018, **428**, 140.

31 M. A. Haque, A. D. Sheikh, X. Guan and T. Wu, *Adv. Energy Mater.*, 2017, **7**, 1602803.

32 J. H. Kim, P. W. Liang, S. T. Williams, N. Cho, C. C. Chueh, M. S. Glaz, D. S. Ginger and A. K. Jen, *Adv. Mater.*, 2015, **27**, 695–701.

33 F. Zhang, X. Yang, M. Cheng, W. Wang and L. Sun, *Nano Energy*, 2016, **20**, 108–116.

34 H. H. Tsai, W. Y. Nie, J. C. Blancon, C. C. S. Toumpos, R. Asadpour, B. Harutyunyan, A. J. Neukirch, R. Verduzco, J. J. Crochet, S. Tretiak, L. Pedesseau, J. Even, M. A. Alam, G. Gupta, J. Lou, P. M. Ajayan, M. J. Bedzyk, M. G. Kanatzidis and A. D. Mohite, *Nature*, 2016, **536**, 312–316.

35 Y. Liao, H. Liu, W. Zhou, D. Yang, Y. Shang, Z. Shi, B. Li, X. Jiang, L. Zhang, L. N. Quan, R. Quintero-Bermudez, B. R. Sutherland, Q. Mi, E. H. Sargent and Z. Ning, *J. Am. Chem. Soc.*, 2017, **139**, 6693–6699.

36 C. C. Stoumpos, C. M. M. Soe, H. Tsai, W. Nie, J.-C. Blancon, D. H. Cao, F. Liu, B. Traore, C. Katan, J. Even, A. D. Mohite and M. G. Kanatzidis, *Chem*, 2017, **2**, 427–440.

37 S. Yang, Y. Wang, P. Liu, Y.-B. Cheng, H. J. Zhao and H. G. Yang, *Nat. Energy*, 2016, **1**, 15016.

38 F. Wang, W. Geng, Y. Zhou, H. H. Fang, C. J. Tong, M. A. Loi, L. M. Liu and N. Zhao, *Adv. Mater.*, 2016, **28**, 9986–9992.

39 Y. Kawamura, H. Mashiyama and K. Hasebe, *J. Phys. Soc. Jpn.*, 2002, **71**, 1694–1697.

40 H. Zhang, H. Huang, K. Haule and D. Vanderbilt, *Phys. Rev. B: Condens. Matter Mater. Phys.*, 2014, **90**, 165143.

41 S. Piskunov, E. A. Kotomin, E. Heifets, J. Maier, R. I. Eglitis and G. Borstel, *Surf. Sci.*, 2005, **575**, 75–88.

42 M. M. Lee, J. Teuscher, T. Miyasaka, T. N. Murakami and H. J. Snaith, *Science*, 2012, **338**, 643–647.

43 Q. Zhou, Q. Chen, Y. Tong and J. Wang, *Angew. Chem., Int. Ed.*, 2016, **55**, 11437–11441.

44 N. Balakrishnan, Z. R. Kudrynskyi, E. F. Smith, M. W. Fay, O. Makarovsky, Z. D. Kovalyuk, L. Eaves, P. H. Beton and A. Patane, *2D Mater*, 2017, **4**, 025043.

45 H. J. Terpstra, R. A. Degroot and C. Haas, *Phys. Rev. B: Condens. Matter Mater. Phys.*, 1995, **52**, 11690–11697.

46 M. Vithal, P. Nachimuthu, T. Banu and R. Jagannathan, *J. Appl. Phys.*, 1997, **81**, 7922–7926.

47 G. Kresse and J. Hafner, *Phys. Rev. B: Condens. Matter Mater. Phys.*, 1993, **47**, 558–561.

48 G. Kresse and J. Furthmuller, *Phys. Rev. B: Condens. Matter Mater. Phys.*, 1996, **54**, 11169–11185.

49 J. P. Perdew, K. Burke and M. Ernzerhof, *Phys. Rev. Lett.*, 1996, **77**, 3865–3868.

50 S. Grimme, J. Antony, S. Ehrlich and H. Krieg, *J. Chem. Phys.*, 2010, **132**, 154104.

51 G. J. Martyna, M. L. Klein and M. Tuckerman, *J. Chem. Phys.*, 1992, **97**, 2635–2643.

52 G. Henkelman, B. P. Uberuaga and H. Jonsson, *J. Chem. Phys.*, 2000, **113**, 9901.

2282 | *J. Mater. Chem. A*, 2019, **7**, 2275–2282

This journal is © The Royal Society of Chemistry 2019